Journal of Membrane Science 582 (2019) 182–193

Contents lists available at ScienceDirect

Journal of Membrane Science

journal homepage: www.elsevier.com/locate/memsci

Gas separation properties of polybenzimidazole/thermally-rearranged polymer blends

Joshua D. Moon, Alexander T. Bridge, Colton D'Ambra, Benny D. Freeman*, Donald R. Paul

John J. McKetta Jr. Department of Chemical Engineering, The University of Texas at Austin, 2501 Speedway, Austin, TX 78712, USA

ARTICLE INFO

Keywords:
Polybenzimidazole
Polyimide
Thermal rearrangement
Polymer blend
Gas transport

ABSTRACT

Polybenzimidazole (PBI) is highly selective for H_2 removal from mixtures with CO_2, but it exhibits low gas permeabilities. Celazole® PBI was blended with more permeable HAB-6FDA-CI, an *ortho*-functional thermally rearrangeable polyimide, to improve its gas permeabilities while attempting to maintain high selectivity. A compatibilizer, 1-methylimidazole, enhanced phase dispersion when added to the casting solutions. Films containing 20–40 wt% polyimide exhibited a matrix-droplet morphology as observed by scanning and transmission electron microscopy. Heat treatment at 400 °C under inert atmosphere thermally rearranged the polyimide in the blends. After heat treatment, H_2/CO_2 selectivities at 35 °C doubled for Celazole® and 20–33 wt% polyimide compatibilized blends, exceeding the 2008 upper bound. Simultaneous increases in both H_2 permeability and H_2/CO_2 selectivity were observed after heat treatment for the 33/67 wt% HAB-6FDA-CI/Celazole® compatibilized blend, which exhibited over twice the H_2 permeability of Celazole® and similar selectivity. Heat treatment reduced free volume and induced para-crystallinity in the PBI phase of the blends as evidenced by x-ray scattering. Thermally treated blend films were mechanically flexible and exhibited elastic moduli and tensile strengths similar to Celazole®, despite having low elongation at break.

1. Introduction

Polybenzimidazoles (PBIs) have recently been studied for use as gas separation membranes for aggressive, high-temperature applications such as hydrogen separations due to their high chemical and thermal stability [1–6]. Most PBI gas permeation studies have targeted H_2/CO_2 separation, since H_2 removal from gas mixtures with CO_2 is integral to pre-combustion carbon capture from streams exiting water-gas shift reactors [2,6–9]. This process is a crucial route for producing H_2 for chemical applications [2,7]. The most commonly studied PBI is a commercial polymer known as Celazole®, the structure of which is shown in Fig. 1A. At low temperatures (e.g., 35 °C), Celazole® has H_2/CO_2 separation performance near the 2008 Robeson upper bound [10,11]. At elevated temperatures, up to 250 °C, Celazole® exhibits separation properties far in excess of the 35 °C upper bound due to increased permeabilities [2].

However, at ambient temperatures, the permeabilities of Celazole® are very low (e.g., 3 Barrer for H_2 at 35 °C) and lie at the low permeability end of the upper bound [11]. Significant opportunity exists for improving PBI gas permeabilities, which would increase the throughput of PBI gas separation membranes. Increasing PBI permeabilities while maintaining good selectivities for gas pairs such as H_2/CO_2 could make this technology competitive for pre-combustion carbon capture applications and emerging applications such as H_2/CH_4 and H_2/hydrocarbon separations.

There are several reported strategies for improving PBI permeabilities. One approach is to change the chemical structure of PBI by incorporating flexible sulfone groups [12], bulky fluorinated or phenylindane groups [2], or by functionalizing the imidazole nitrogen with bulky alkyl or aromatic groups [5,13]. Such materials all suffer from the intrinsic trade-off between permeability and selectivity and do not surpass the 2008 H_2/CO_2 upper bound. Another strategy is to form mixed-matrix or nanocomposite membranes using porous fillers such as zeolitic imidazolate frameworks (ZIFs) [14–18]. Some of these materials surpass the upper bound but are complicated by additional factors necessary to produce nanocomposite membranes, including ZIF aggregation and synthesis of expensive nanoparticles at large scales. A third strategy is to blend PBI with a more permeable polymer such as a polyimide [19–27] or sulfonated polyphenylsulfone [28], or to copolymerize Celazole® with a more permeable fluorinated PBI [29].

This study seeks to improve the permeabilities of PBIs by blending Celazole® with a more permeable, *ortho*-functional polyimide. These blends are then heat treated to further increase their permeabilities by taking advantage of the thermal rearrangement ("TR") reaction of *o*-

* Corresponding author.
E-mail address: freeman@che.utexas.edu (B.D. Freeman).

https://doi.org/10.1016/j.memsci.2019.03.067
Received 31 August 2018; Received in revised form 21 March 2019; Accepted 23 March 2019
Available online 25 March 2019

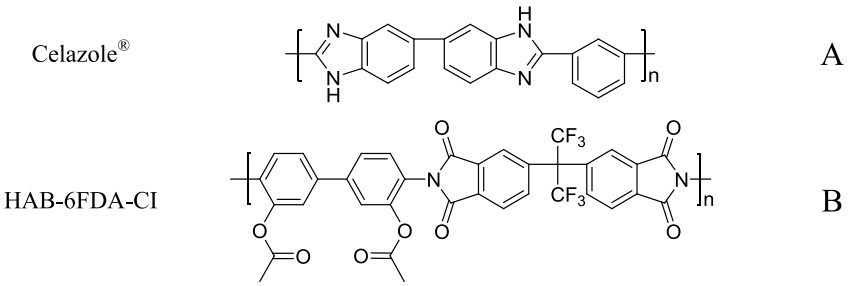

Fig. 1. Molecular structures of (A) Celazole® PBI and (B) HAB-6FDA-CI.

functional polyimides to form polybenzoxazoles, which significantly increases their permeabilities [9,30–37]. The chosen polyimide is HAB-6FDA-CI, which contains acetate groups *ortho* to the imide nitrogen (Fig. 1B). An immiscible PBI/polyimide blend where PBI is the continuous phase and polyimide is the dispersed phase could potentially maintain high selectivities due to the PBI phase while having increased permeabilities resulting from the polyimide phase. In the present study, however, an increase in both permeabilities and selectivities after heat treatment was observed, presumably due to changes in structural order in the PBI phase. PBI/polyimide blends were characterized by thermogravimetric analysis with mass spectroscopy, gel fraction and density measurements, scanning electron microscopy, transmission electron microscopy, scanning transmission electron microscopy with energy-dispersive x-ray spectroscopy, wide and small angle x-ray scattering, and tensile mechanical tests. Pure gas H_2, CH_4, N_2, O_2, and CO_2 permeabilities at 35 °C were measured for untreated and heat treated blends with compositions ranging from 20 to 80% HAB-6FDA-CI.

2. Experimental

2.1. Materials

Celazole® was purchased as a dope solution (S26) from PBI Performance Products Inc. that contains 26% polymer by weight in *N,N*-dimethylacetamide (DMAc) with 1.5 wt% LiCl added to improve polymer solubility. HAB-6FDA-CI was synthesized and purified as described previously following a chemical imidization ("CI") route [38]. DMAc (99.8%, anhydrous) and 1-methylimidazole (99%) were purchased from Sigma-Aldrich and used as received. Deionized water was generated using a Millipore RiOs and A10 purification system. Ultra high purity gases were purchased from Airgas. Structures of Celazole® and HAB-6FDA-CI are shown in Fig. 1.

2.2. Solution casting of polymer films

2.5 wt% solutions of Celazole® and HAB-6FDA-CI were prepared in *N,N*-dimethylacetamide (DMAc). Each polymer was weighed and added to a glass scintillation vial, to which a corresponding amount of DMAc was added to form a 2.5 wt% solution. The solutions were stirred at room temperature overnight or until completely dissolved. A 2.5 wt% solution of 1-methylimidazole in DMAc was likewise prepared.

Solution blending was performed using a procedure adapted from Panapitiya et al. [22] For blends without 1-methylimidazole, PBI solution was weighed into a glass scintillation vial. Polyimide solution was slowly added, then the solution was stirred overnight at room temperature. For blends with 1-methylimidazole, 2.5 wt% 1-methylimidazole solution in DMAc was weighed into a glass scintillation vial. A third of the corresponding amount of PBI solution was added, the mixture was stirred for 30 min at room temperature, and then the mixture was sonicated for 30 min at room temperature using a sonication bath. This cycle was repeated two more times for the remaining two thirds of the PBI solution. Finally, the polyimide solution was added dropwise, and the resulting solution was stirred overnight at room temperature.

For unblended PBI or polyimide films with 1-methylimidazole additive, 1-methylimidazole solution in DMAc was weighed into a glass scintillation vial. A third of the corresponding amount of PBI or polyimide solution was added, then the mixture was stirred and sonicated as above. The remaining thirds of the solution were also added in sequence, each followed by 30 min of stirring and 30 min of sonication. The final solutions were stirred overnight at room temperature.

Prior to film casting, the solutions were passed through a 0.45 µm PTFE filter, sonicated for 30 min at room temperature, and then poured onto a clean glass plate inside a glass ring. The plate was placed in a vacuum oven equipped with a liquid nitrogen trap. The solvent was evaporated by pulling full vacuum on the solution overnight at room temperature, then at 60–80 °C for 4 h, then at 100 °C for 1 h [12]. Solid films were delaminated using a razor blade and deionized (DI) water, and they were subsequently boiled in DI water for 4 h to remove residual DMAc present in the PBI dope. Solvent removal was verified using TGA-MS. Films were blotted dry, placed between two glass plates wrapped in aluminum foil, then dried at 140–150 °C under full vacuum in a vacuum oven for 24 h.

2.3. Heat treatment (thermal rearrangement) process

Heat treatment of film samples was performed using a previously described procedure for thermally rearranging polyimides (the "TR 400" procedure in Sanders et al.) [31]. Small sections of films (approximately 4 cm^2 in area) were cut and placed between two ceramic plates separated by stainless steel washers. The plates were loaded into a Carbolite Split-Tube Furnace equipped with a quartz tube. A UHP nitrogen purge of 900 mL/min at ambient pressure maintained an inert environment around the samples during heat treatment. The samples were heated from ambient temperature to 300 °C at a ramp rate of 5 °C/min and held for 1 h, then heated to 400 °C at a ramp rate of 5 °C/min and held for 1 h. The sample was then cooled to ambient temperature under nitrogen flow at a rate not exceeding 10 °C/min. After removal from the oven, all of the samples except pure Celazole® appeared darker in color, particularly those with higher polyimide fractions.

2.4. Thermogravimetric analysis with mass spectrometry (TGA-MS)

Thermal mass loss and decomposition products were determined using TGA-MS. Measurements were performed using a TA Instruments Q500 TGA connected to a Pfeiffer Vacuum Thermostar mass spectrometer. Samples were degassed at 50 °C in the TGA for at least 30 min prior to beginning the temperature ramp to remove sorbed water and oxygen from the system. The TGA temperature ramp was 10 °C/min from 50 to 800 °C with UHP nitrogen purge. The mass spectrometer simultaneously recorded decomposition products using a Secondary Electron Multiplier (SEM) detector set to continuously scan 1–100 amu with a 100 ms dwell time.

2.5. Gel fraction measurement

Samples of 20/80 and 33/67 wt% HAB-6FDA-CI/Celazole® blends with 1-methylimidazole additive were dried at 150 °C under full vacuum for 19 h. The vacuum oven was purged with dry air via a Drierite column, then the samples were quickly removed and weighed in sealed glass vials to avoid moisture uptake from the atmosphere. Samples were then placed in Soxhlet extraction columns with DMAc heated under reflux for 45 h. The samples were removed from the Soxhlet extractors and dried under full vacuum at 150 °C for 30 h to remove DMAc solvent. The vacuum oven was then purged with dry air, and the samples were removed and weighed in sealed glass vials. The gel fraction (i.e., insoluble fraction) was calculated as the final film mass divided by the initial film mass.

2.6. Density measurement

PBI can absorb significant amounts of water, which could influence density measurements [39]. Therefore, the following procedure was used to minimize water sorption in samples prior to density measurement. Untreated and heat treated PBI samples cast with 1-methylimidazole were cut and placed in stainless steel chambers built from Swagelok VCR fittings equipped with isolation valves. The cells were placed inside an oven under full vacuum at 150 °C for 24 h with valves open to allow samples to dry. This drying procedure is sufficient to remove all of the sorbed water from the samples [39]. The oven was purged with air dried via two Drierite® columns in series and opened, then the isolation valves were immediately closed to prevent humid ambient air from entering the cells. The cells were transferred to a glove box purged with nitrogen which was dried to a humidity of < 0.1% measured by a digital hygrometer (Fisher Scientific, ± 2% RH accuracy). The cells were opened, and film densities were measured using a balance and density kit (Mettler Toledo) inside the dry box [40]. The buoyant liquid was *n*-heptane, which has negligible sorption in PBIs over the timescale of the density measurements [39].

2.7. Pure gas permeability measurement

Films of uniform thickness were epoxied to brass support disks using Master Bond EP46HT-2 epoxy with a glass fiber filter backing to protect the films. Film thicknesses were measured using digital calipers (Mitutoyo, ± 1 μm resolution) and ranged from 10 to 30 μm. The epoxy was cured in air by placing the samples in an oven for 3 h at around 140 °C followed by 3 h at 180 °C. Samples were loaded into a modified high pressure Millipore filter holder (Cat. No. XX4504700, Millipore), which served as the permeation cell, equipped with isolation valves on the upstream and downstream sides of the cell. The filter holder was placed in a vacuum oven with both valves open and dried at 150 °C under full vacuum for 24 h to remove any sorbed water from the samples. The oven was cooled under vacuum and purged with dry air via Drierite columns. The oven was opened, and the valves were quickly closed to minimize exposure to ambient humidity. The cell was transferred to a temperature-regulated constant-volume, variable-pressure permeation system [41], connected, and degassed overnight at 35 °C to remove any sorbed gas from the sample.

The permeabilities of H_2, CH_4, N_2, O_2, and CO_2 were measured at 35 °C at pressures between 2 and 10 atm. The downstream pressure rise was measured with an MKS Baratron with a 10 Torr range, and the upstream pressure was measured with a Honeywell STJE transducer. N_2 and CH_4 were not tested for some membranes due to their low fluxes, which in some cases were at or below instrument sensitivity.

2.8. Scanning electron microscopy (SEM)

Cross-sections of polymer films were formed by cryofracturing. Small pieces of film were immersed in liquid nitrogen for 60 s, then quickly broken in the nitrogen with flat tweezers. Samples were sputter-coated for 60 s with a 60:40 Au/Pt alloy. Cross-sections were imaged using a Hitachi S5500 SEM at 15 kV and 5 mA.

2.9. Transmission electron microscopy (TEM) and scanning transmission electron microscopy with energy-dispersive x-ray spectroscopy (STEM/EDS)

TEM samples were prepared by ultramicrotoming. Small pieces of film were potted in epoxy resin (Epofix™ cold-setting embedding resin) that was cured overnight. An RMC PowerTome ultramicrotome was used to cut 60–70 nm thick sections, which were placed on copper TEM grids (Pelco®). Samples were imaged in a Jeol 2010F TEM at 120 kV in both TEM and STEM mode. The lower voltage was used to minimize damage to the polymer from the electron beam. EDS was used in STEM mode to provide elemental analysis for nitrogen, oxygen, and fluorine.

2.10. Wide and small angle x-ray scattering (WAXS and SAXS)

Wide and small x-ray scattering were measured for small film samples in a Xenocs Ganesha small angle scattering instrument equipped with a moveable Dectris 300k detector to record both wide and small angle scattering. The instrument was equipped with a microfocus CuKα source and was operated at 50 kV and 0.6 mA. Scattering data were corrected for incident beam intensity by directly measuring I_0 on the Dectris detector. Data were also corrected for sample thicknesses to yield absolute scattering intensities. SAXSGUI (Rigaku Innovative Technologies, Inc. and JJ X-ray Systems ApS), a manufacturer supplied software utility, was used to provide corrections and to convert 2-D detector data into intensities as a function of scattering angle. WAXS data for Celazole® cast with 1-methylimidazole without heat treatment were reported previously [42].

2.11. Mechanical properties

Mechanical properties of pure Celazole® and heat treated blends were determined using a Shimadzu Autograph AGS-X 500N tensile testing instrument. Films with thicknesses of 10–20 μm were cut before heat treatment using a microtensile dogbone-shaped die with a width of 5 mm and gauge length of 22 mm (ASTM D1708-13). Die cut samples were heat treated using the TR 400 process described above. Since the samples shrunk slightly after heat treatment, the width and gauge length of the treated samples were determined by scanning the samples with a digital scanner and determining the average width and gauge length using ImageJ software. Thicknesses were measured after heat treatment via digital calipers (Mitutoyo, ± 1 μm resolution). The crosshead speed of the tensile test was set to 1 mm/min. Ultimate tensile strength was determined as the maximum stress observed during the test.

3. Results and discussion

3.1. Blend morphology

Blends of HAB-6FDA-CI and Celazole® were prepared at compositions ranging between 20 and 80 wt% polyimide. Blends containing 20 wt% polyimide did not show macroscopic phase separation under optical microscopy, but they were semitransparent, indicating immiscibility. However, as shown in Fig. 2, films containing 33–67 wt% polyimide showed macroscopic phase separation. These results stimulated a search for methods to improve the compatibility and mixing of the PBI and polyimide.

A previous study reported that 2-methylimidazole could compatibilize 50/50 wt% immiscible blends of Celazole® and a 6FDA-DAM:DABA(3:2) copolyimide [22]. It was reported that 2-methylimidazole localized at the interface of the PBI and copolyimide phases, decreasing interfacial tension during solution casting, which resulted in

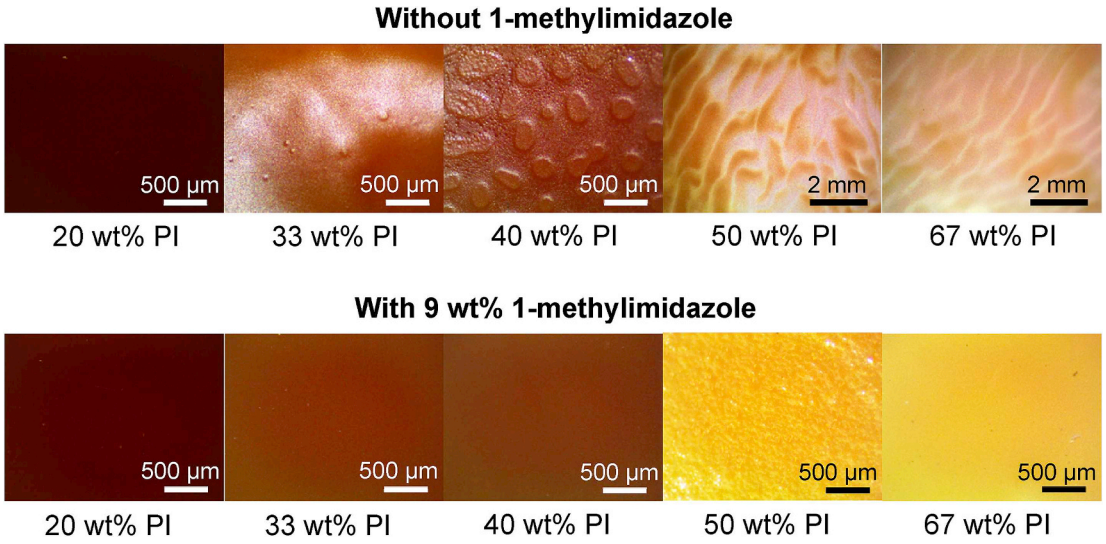

Fig. 2. Optical microscope images of HAB-6FDA-CI/Celazole® blends without (top) and with (bottom) 9 wt% 1-methylimidazole additive. Polyimide (PI) weight percentages represent the amount in the final films after 1-methylimidazole is removed.

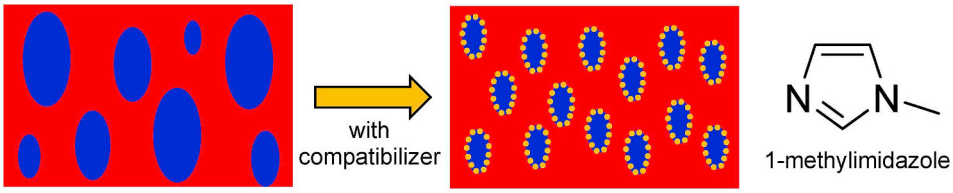

Fig. 3. Illustration of potential blend morphology changes when a small molecule compatibilizer (e.g., 1-methylimidazole or 2-methylimidazole; yellow circles) localizes at the interface between a continuous matrix of PBI (red) and dispersed domains of polyimide (blue) [22]. The chemical structure of 1-methylimidazole is shown on the right. (For interpretation of the references to color in this figure legend, the reader is referred to the Web version of this article.)

better dispersion of the polymers in the resulting blend (cf., Fig. 3) [22,23]. FTIR indicated that 2-methylimidazole interacted via hydrogen bonding with –OH groups on the copolyimide carboxyl moieties. While no evidence supported the creation of hydrogen bonding between 2-methylimidazole and the PBI, it was hypothesized that hydrophobic or π-π interactions between 2-methylimidazole and PBI could result in 2-methylimidazole localizing at the interface of the two polymer phases.

Yousfi et al. observed similar phenomena in a study employing phosphonium-based ionic liquids (ILs) as compatibilizers for 80/20 wt % immiscible blends of polypropylene (PP) and polyamide (PA) [43]. The authors asserted that, at low (1 wt%) loadings of IL, the dispersed PA droplets decreased in diameter from 27 to 1–2 μm, resulting from preferential migration of the IL to the interface between the two phases [43]. Once at the interface, the IL acted as a "barrier" to the coalescence of small PA droplets. Broseta et al. concluded that a solvent or additive with an affinity for two sufficiently immiscible polymer phases in a mixture preferentially locates at their interface, lowering interfacial tension [44]. For larger compatibilizer molecules, such as an AB-type diblock copolymer in immiscible blends of A and B, other studies have claimed that lower interfacial tension results from the tendency of the block copolymer to localize at the boundary between the homopolymer constituents [45,46].

As an attempt to use a similar approach to compatibilize PBI blends, PBI/polyimide blend films were cast with 1-methylimidazole (chemical structure shown in Fig. 3) added to the casting solutions in the present work. It was hypothesized that adding 1-methylimidazole to the casting solutions could help lock in phase morphology during solvent evaporation as glassy films were formed. 9 wt% of 1-methylimidazole was used relative to the total mass of the polymers and additive for all of the compatibilized blends. This composition was chosen as it resulted in better phase dispersion than 5 wt% in a previous study [22]. TGA-MS results, discussed below, indicated that all of the 1-methylimidazole was removed during film preparation and was not present in the final films, which was also observed for previously reported 2-methylimidazole compatibilized blends [22]. 1-methylimidazole has a normal boiling point of 196 °C and is water soluble, so it could potentially be removed during the initial solvent removal step (i.e., evaporation under vacuum at up to 100 °C), during water boiling, or during the 150 °C vacuum drying step. TGA-MS results (provided in the supporting information) did not find evidence of 1-methylimidazole in the films after the initial solvent removal step and before water boiling, suggesting most of the 1-methylimidazole was removed during the initial drying steps as the glassy films were being formed.

Compositions described hereafter will refer to weight fractions of the polymers in the blends after 1-methylimidazole removal (e.g., "20/80 wt% HAB-6FDA-CI/Celazole® compatibilized blends" were initially cast with 18.2 wt% HAB-6FDA-CI, 72.7 wt% Celazole®, and 9.1 wt% 1-methylimidazole). While 1-methylimidazole lacks the hydrogen bond donor site present in 2-methylimidazole, it has a much lower boiling point (196 °C vs. 267 °C) and can be more easily removed during solution casting and film drying protocols. Use of a different compound from 2-methylimidazole reported previously also permits insight into the potential breadth of chemical structures that are useful as small molecule compatibilizing agents.

As shown in Fig. 2, films made with 1-methylimidazole in the casting solution showed qualitatively improved phase dispersion relative to films without 1-methylimidazole and did not show the large scale macroscopic phase separation observed in samples without 1-methylimidazole. All films were semitransparent and, with the exception of the 50/50 wt% HAB-6FDA-CI/Celazole® compatibilized blend, were uniform in optical microscopy. SEM and TEM were employed to further characterize blend morphology. Fig. 4 shows cross-sectional SEM images of 20/80 and 33/67 wt% HAB-6FDA-CI/Celazole® blends

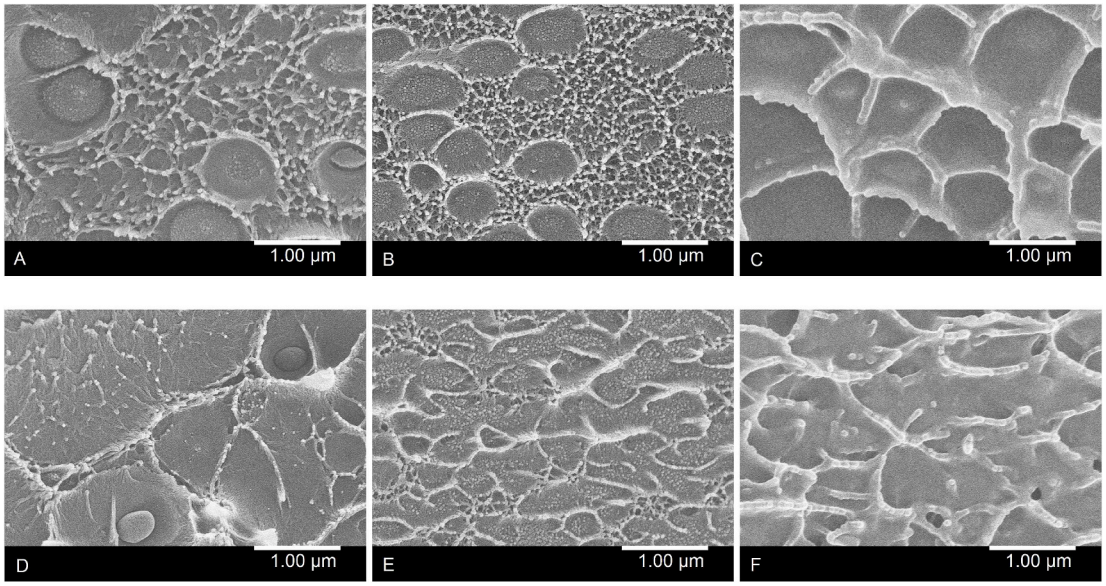

Fig. 4. Cross-sectional SEM images of a 20/80 wt% HAB-6FDA-CI/Celazole® blend (A) without compatibilizer, (B) with compatibilizer, and (C) with compatibilizer after 400 °C heat treatment. Cross-sectional SEM images of a 33/67 wt% HAB-6FDA-CI/Celazole® blend (E) without compatibilizer, (F) with compatibilizer, and (G) with compatibilizer after 400 °C heat treatment.

with and without compatibilizer. Compatibilized blends have a matrix/droplet morphology, where the matrix phase is Celazole® and the dispersed droplets are HAB-6FDA-CI, which was determined by EDS analysis as described in more detail below. Most of the dispersed domains have sub-micron dimensions. It cannot be concluded with certainty that the dispersed domain sizes of the 20/80 wt% HAB-6FDA-CI/Celazole® blends were reduced when the compatibilizer was added (cf., Fig. 4A and B). However, 33/67 wt% HAB-6FDA-CI/Celazole® blends appeared to show smaller, much more uniform dispersion of the polyimide dispersed phase when 1-methylimidazole is added (cf., Fig. 4D and E), consistent with the observed differences in optical microscopy (cf., Fig. 2) and with previous reports of the use of 2-methylimidazole to compatibilize 50/50 wt% PBI/6FDA-DAM:DABA(3:2) blends [22].

The droplet structure of the polyimide phase can be more clearly seen in the TEM image of a 33/67 wt% HAB-6FDA-CI/Celazole® compatibilized blend without heat treatment in Fig. 5A. The white regions on the left sides of some of the droplets are believed to be the electron beam passing through a narrow region where the polyimide phase has slightly separated from the PBI phase, which possibly occurred during microtoming. Alternatively, there may be some void space created around the polyimide phase during casting.

To confirm that the dispersed phase was in fact polyimide, EDS mapping was performed on a small region of a 33/67 wt% HAB-6FDA-CI/Celazole® compatibilized blend film. Fig. 5B–D are elemental maps for nitrogen, oxygen, and fluorine, respectively, and Fig. 5E is a STEM image of the film region used for mapping. The darker regions in Fig. 5B show that the dispersed phase has lower nitrogen content than the surrounding matrix. Likewise, the brighter regions in Fig. 5C indicate that the dispersed phase has higher oxygen content than the surrounding matrix. Since HAB-6FDA-CI has half the nitrogen atoms per repeat unit as Celazole® and HAB-6FDA-CI has 8 oxygen atoms per repeat unit while Celazole® has zero, the dispersed phase must be composed primarily of polyimide, while the matrix phase contains primarily PBI. While a slightly higher fluorine content was observed in the dispersed phase than in the matrix from the polyimide CF_3 groups, the contrast was poor because few x-ray counts were observed, even after running EDS for around 15 min.

We speculate that, like 2-methylimidazole, some 1-methylimidazole could localize at the interface between Celazole® and HAB-6FDA-CI domains during casting, reducing interfacial tension and dispersed

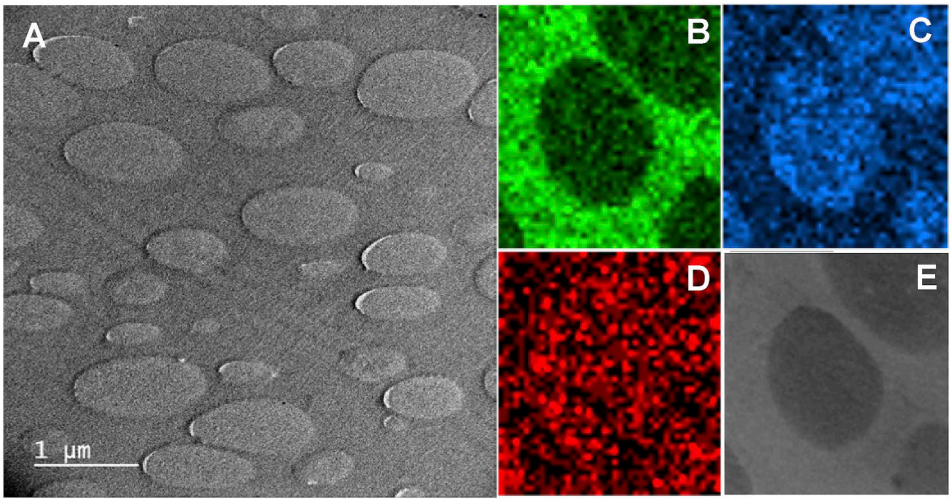

Fig. 5. (A) TEM image of a 33/67 wt% HAB-6FDA-CI/Celazole® compatibilized blend without heat treatment. (B–D) EDS map for nitrogen (B), oxygen (C), and fluorine (D) for a 33/67 wt% HAB-6FDA-CI/Celazole® compatibilized blend. Bright regions indicate areas with high x-ray counts that indicate the abundance of the specified element. (E) STEM image of film area used for EDS mapping. Scale bars are not available for (B–E) as the camera was not fully calibrated for STEM mode.

polymer domain size and improving uniformity of dispersion (cf., Fig. 3) [22]. A majority of the compatibilizer likely remained dispersed throughout one or both phases, depending on how the compatibilizer interacts with each polymer. A monolayer of 1-methylimidazole between the polymer phases could only account for approximately 1% of total compatibilizer added to the blends (see supporting information for calculation details). A similar observation has been made for excess (10–20 wt%) phosphonium ionic liquid compatibilizers in 80/20 wt% PP/PA blends, where ionic liquids preferentially migrated into the phase for which the anion displayed a higher affinity [43]. The localization of 1-methylimidazole to the phase interface, however, remains simply speculation at the present time and is primarily based on previous observations in the literature. The thermodynamics of this four component system consisting of two polymers, a solvent, and a compatibilizer are complex, and a more complete understanding of how these blend morphologies are formed necessitates future study that is beyond the scope of the present work.

400 °C heat treatment of compatibilized blends did not appear to significantly affect their morphology, as they retained a phase separated structure with similar dispersed domain sizes (cf., Fig. 4). Additional SEM images, including images for blends containing 50–80 wt% HAB-6FDA-CI, can be found in the supporting information.

3.2. Heat treatment

TGA was used to estimate conversion of polyimide to polybenzoxazole in compatibilized blends. Compatibilized blend films containing 20, 33, and 40 wt% HAB-6FDA-CI were tested before and after 400 °C heat treatment in the tube furnace, and the results for a 20 wt% polyimide compatibilized blend are presented in Fig. 6. Additional results for other compositions are in the supporting information. The mass loss was normalized to the mass of the samples in the TGA at 150 °C due to water loss from the PBI phase, since PBI is known to strongly sorb water, which requires elevated temperatures to remove [39].

Acetate-functionalized HAB-6FDA-CI is known to undergo thermal rearrangement between about 300 and 450 °C by first losing acetate groups in the form of ketene as the *ortho*-position acetate groups convert to *ortho*-position hydroxyl groups [38,47]. The hydroxyl-functionalized polyimide then rearranges to a polybenzoxazole structure through loss of CO_2 [38,47]. Blends that had not been thermally treated at 400 °C for 1 h showed a 4–7% mass loss between 250 and 450 °C that corresponded to the expected rearrangement process. Samples that had already undergone 400 °C heat treatment in the tube furnace, however, showed no mass loss in this region (cf., Fig. 6). Analysis of decomposition products via mass spectrometry shows loss of ketene groups (41 amu) and CO_2 (44 amu) in this region for the untreated blends (see supporting information), consistent with polyimide conversion to polybenzoxazole. FTIR corroborates the formation of polybenzoxazole in the polyimide phase after heat treatment, which is discussed in the supporting information. No mass fragments associated with DMAc (87 amu) or 1-methylimidazole (82 amu) were observed, so both solvent and compatibilizer were removed during the film formation process (cf., Fig. S8). TGA-MS scans run on films removed from the casting oven after the 100 °C solvent evaporation step and before boiling in water and the subsequent 150 °C drying step also did not show mass fragments associated with 1-methylimidazole despite some DMAc still being present, indicating the 1-methylimidazole is likely removed during the initial solvent removal steps (see supporting information).

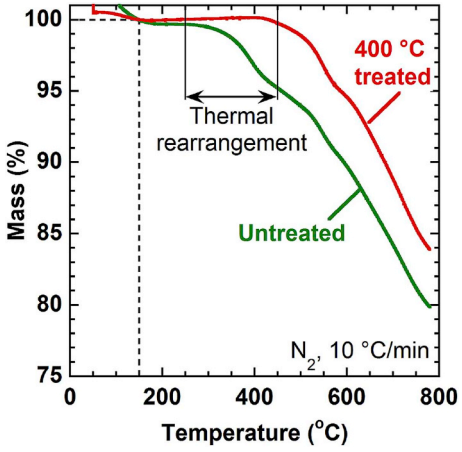

Fig. 6. TGA thermograms of 20/80 wt% HAB-6FDA-CI/PBI compatibilized blend before (green curve) and after (red curve) 400 °C heat treatment in tube furnace. Scans were run under nitrogen at a ramp rate of 10 °C/min. Mass percentages were normalized based on sample dry mass at 150 °C. (For interpretation of the references to color in this figure legend, the reader is referred to the Web version of this article.)

The conversion of polyimide to polybenzoxazole in the blends can be estimated by determining the difference in mass loss in the 250–450 °C region between the untreated and heat treated samples. If all of the mass loss between 250 and 450 °C is due to the polyimide phase undergoing thermal rearrangement, the conversion of polyimide to polybenzoxazole can be calculated since the weight fraction of polyimide in the films is known. Celazole® is thermally stable to above 550 °C, so none of the mass loss in the 250–450 °C region is believed to be due to PBI decomposition [1,4]. Finally, the conversion to polybenzoxazole can be calculated assuming 100% conversion corresponds to 24.3% mass loss of the polyimide [47]. Details of this calculation are provided in the supporting information (Table S1). Compatibilized blends containing 20, 33, and 40 wt% HAB-6FDA-CI were estimated to undergo 64%, 58%, and 56% TR conversion of the polyimide, respectively. Since pure HAB-6FDA-CI undergoes 60% conversion at the same heat treatment conditions, the presence of the PBI matrix does not appear to hinder thermal rearrangement of the polyimide [38].

3.3. Gas transport properties

Polymer blend gas transport properties strongly depend on polymer miscibility and blend morphology [48–50]. Fig. 7 illustrates theoretical transport properties of Celazole®/HAB-6FDA-CI blends plotted on the 2008 H_2/CO_2 upper bound (see supporting information for details) [10]. If the two polymers are miscible, blend permeability would be expected to follow a logarithmic average of the permeabilities of the two components weighted by their volume fractions, leading to a linear trade-off between the two polymers on the upper bound (cf., dashed purple line in Fig. 7) [48,50]. Consequently, miscible blends of two polymers would not surpass the upper bound for a given gas pair unless one of the polymers was already above the upper bound.

However, if the two polymers are immiscible, blend permeability is strongly dependent on the morphology of the two phases and can be described by various models [48–50]. In the simplest case, where one polymer forms uniformly distributed, spherical dispersions in a continuous matrix of the second polymer, the transport behavior can be described by the Maxwell model [48–50]. This model predicts the selectivity of the phase separated blend to be primarily dictated by the selectivity of the continuous phase. The dispersed phase would then act either as a more permeable filler, increasing the blend permeability relative to that of the matrix phase polymer (cf., solid red curve in Fig. 7), or as a less permeable filler, decreasing the blend permeability relative to that of the matrix phase polymer (cf., dashed blue curve in Fig. 7).

Pure gas permeabilities for H_2, CH_4, N_2, O_2, and CO_2 at 35 °C and 10 atm in untreated and heat treated blends compatibilized with 9 wt% 1-methylimidazole are shown in Fig. 8A and B, respectively. Some data are absent, since N_2 and CH_4 permeabilities were too low to measure for some films below 50 wt% polyimide. Fig. 9 presents the transport

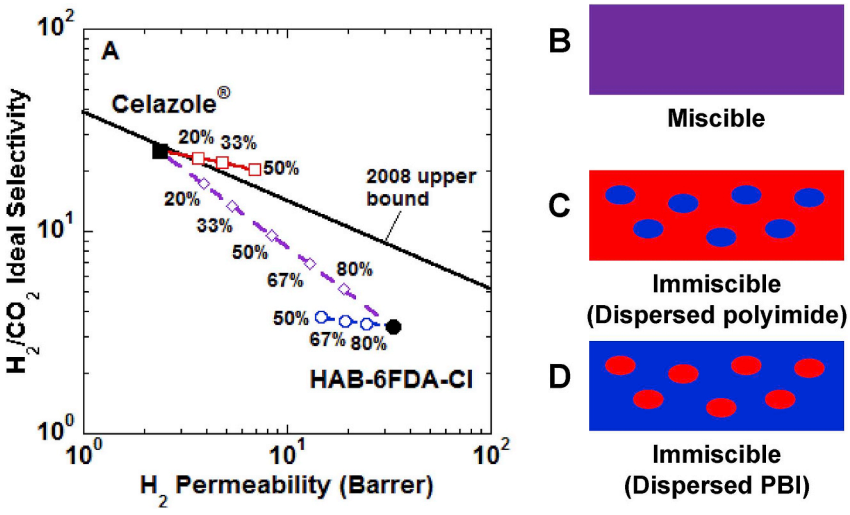

Fig. 7. (A) Theoretical transport properties for Celazole®/HAB-6FDA-CI blends plotted on H_2/CO_2 upper bound (black solid line represents 2008 upper bound) [10]. Additive (miscible) model values are purple unfilled diamonds and dashed line (graphic B) [48,50], Maxwell (immiscible) model values for blends with continuous Celazole® phase are red unfilled squares and solid line (graphic C) [48–50], and Maxwell model values for blends with continuous HAB-6FDA-CI phase are blue unfilled circles and dashed line (graphic D) [48–50]. Percentages are volume percent of HAB-6FDA-CI chosen arbitrarily for this example. Permeabilities of pure Celazole® (filled black square) and HAB-6FDA-CI (filled black circle) used in calculations are from the literature [11,31]. (B–D) Illustrations of miscible blends and immiscible blends with dispersed polyimide or PBI. (For interpretation of the references to color in this figure legend, the reader is referred to the Web version of this article.)

properties of samples considered in this study on the 2008 H_2/CO_2 upper bound [10]. Permeability values are recorded in the supporting information. Celazole® cast with 9 wt% 1-methylimidazole had higher permeabilities and lower selectivities than Celazole® cast without compatibilizer (e.g., H_2 permeability of 3.7 Barrer vs. 2.4 Barrer and H_2/CO_2 selectivity of 17 vs. 27) [11]. When 1-methylimidazole is removed during casting, it may leave behind additional free volume in the resulting glassy film, resulting in somewhat higher permeabilities and lower selectivities. Films cast without 1-methylimidazole were also dried at slightly higher temperatures (i.e., 190 °C), which may have contributed to more thermal annealing and densification. In contrast, HAB-6FDA-CI cast with 9 wt% 1-methylimidazole had slightly lower permeabilities and higher selectivities than a film of HAB-6FDA-CI without compatibilizer (e.g., H_2 permeability of 24 Barrer vs. 28 Barrer and H_2/CO_2 selectivity of 4.2 vs. 3.7), which was prepared similarly to the film with 1-methylimidazole. Presently, it is unknown why this phenomenon occurs. Both of these films showed lower permeabilities and higher selectivities than HAB-6FDA-CI previously reported in the literature, which was cast from DMAc and underwent drying at 200 °C overnight (H_2 permeability of 38 Barrer and H_2/CO_2 selectivity of 3.2) [31].

Permeabilities and selectivities of 20/80 and 33/67 wt% HAB-6FDA-CI/Celazole® compatibilized blends without heat treatment were similar to those of pure Celazole® cast with 1-methylimidazole, with the 33% polyimide blend showing slightly higher permeabilities and slightly lower selectivities. These results are consistent with the blends

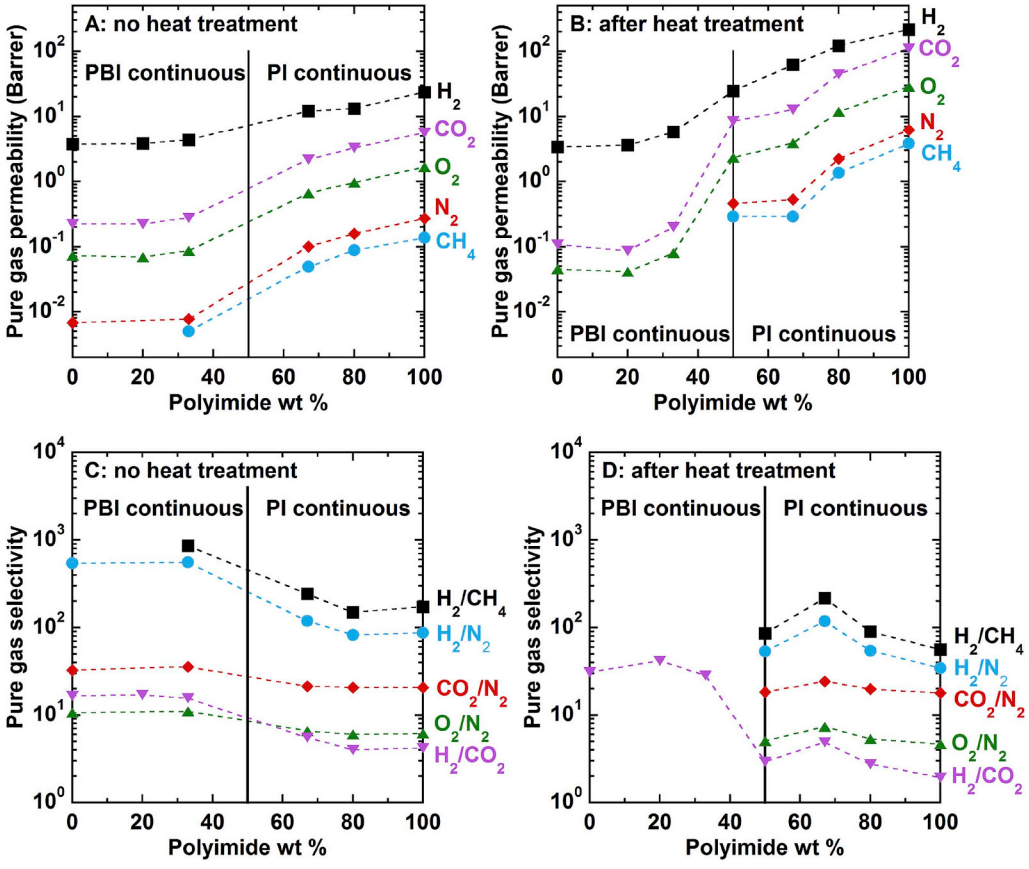

Fig. 8. (A–B) Pure gas permeabilities at 35 °C and 10 atm in compatibilized blends at different weight fractions of polyimide (PI) in the final films (i.e., after 1-methylimidazole is removed but before thermal treatment) (A) before heat treatment and (B) after 400 °C heat treatment in tube furnace. N_2 and CH_4 permeabilities were too low to measure for heat treated films with less than 50 wt% HAB-6FDA-CI. (C–D) Pure gas selectivities at 35 °C and 10 atm in compatibilized blends (C) before heat treatment and (D) after 400 °C heat treatment in tube furnace. The vertical line denotes the approximate composition where phase inversion occurs. Error bars are smaller than the symbols.

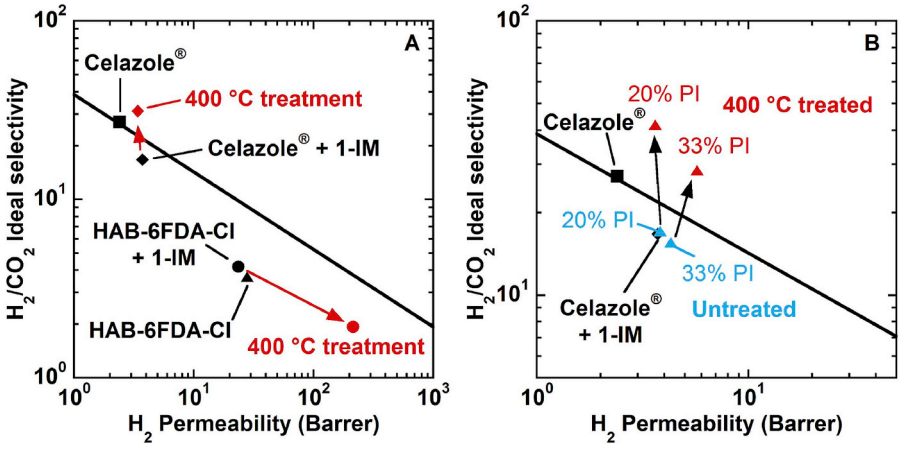

Fig. 9. (A) H_2/CO_2 upper bound for Celazole® and HAB-6FDA-CI pure polymers cast with 1-methylimidazole (1-IM) with and without heat treatment at 400 °C. Untreated Celazole® without 1-IM was measured previously and was prepared via solution casting from DMAc with subsequent 190 °C drying to remove moisture [11]. (B) H_2/CO_2 upper bound plot for 20/80 and 33/67 wt% HAB-6FDA-CI/Celazole® blends compatibilized with 1-IM with and without heat treatment at 400 °C. All measurements were performed at 35 °C and 10 atm. Solid lines represent the 2008 upper bound [10].

having PBI as the continuous phase. A discontinuity in permeability and selectivity occurred at compositions between 33 and 67 wt% HAB-6FDA-CI (cf., Fig. 8), indicating phase inversion occurred at some intermediate composition (i.e., the continuous phase changed from PBI to polyimide) [50–52]. The permeabilities of compatibilized 67 and 80 wt % HAB-6FDA-CI blends were somewhat lower than pure HAB-6FDA-CI cast with 1-methylimidazole, which was expected since the PBI dispersed phase is acting as a low permeability filler.

After heat treatment at 400 °C, the H_2 permeability of Celazole® cast with 1-methylimidazole was relatively unchanged (3.4 Barrer vs. 3.7 Barrer), but the O_2 and CO_2 permeabilities were lower, resulting in an increase in H_2/CO_2 selectivity from 17 to 31. A similar increase in selectivity was previously observed by Perez et al. for Celazole® dried at 300 °C under vacuum for one day which had a H_2/CO_2 selectivity of 49 at 5 bar and 35 °C [53]. This was much higher than the H_2/CO_2 selectivity of 18 measured at 5 bar and 35 °C for Celazole® dried at 250 °C [53]. The reason for this behavior is explored in more detail in the following sections. The permeabilities of HAB-6FDA-CI cast with 1-methylimidazole increased by over an order of magnitude after heat treatment, presumably due to the TR reaction, and selectivities were reduced (cf., Fig. 9A). This behavior is consistent with previously observed permeability increases for TR polymers [9,30,31,36]. Compatibilized 67 and 80% HAB-6FDA-CI blends showed a significant increase in permeability (cf., Fig. 8), indicating thermal rearrangement of the continuous polyimide phase contributed strongly to the permeability increase of blends at these compositions.

Unexpectedly, after heat treatment, the 20/80 wt% HAB-6FDA-CI/Celazole® compatibilized blend showed a slight (5%) decrease in H_2 permeability and a 40% and 61% decrease in O_2 and CO_2 permeabilities, respectively (cf., Fig. 8). Consequently, H_2/CO_2 selectivity increased from 17 to 42, which surpassed the 2008 upper bound (cf., Fig. 9B). The 33/67 wt% HAB-6FDA-CI/Celazole® compatibilized blend showed a 32% increase in H_2 permeability after heat treatment and a 28% decrease in CO_2 permeability, resulting in a H_2/CO_2 selectivity of 29 that also surpassed the upper bound. This film had over twice the H_2 permeability of Celazole® while maintaining essentially the same H_2/CO_2 selectivity [11]. While the increase in blend permeabilities was expected from conversion of polyimide to the more permeable thermally-rearranged polybenzoxazole, the simultaneous increase in selectivity was unexpected and required additional investigation.

Gel fraction measurements were performed on heat treated 20/80 and 33/67% HAB-6FDA-CI/Celazole® compatibilized blends to investigate whether there were any additional changes occurring during heat treatment, such as thermally-induced crosslinking. Crosslinking can increase gas selectivity due to restriction of chain mobility that enhances a polymer's size sieving ability, though this typically comes at the expense of reduced permeability [19,51,54]. Gel fractions were 64% and 62% for the 20/80 and 33/67 wt% HAB-6FDA-CI/Celazole® compatibilized blends after heat treatment, respectively. Thus, high temperature treatment induced some degree of insolubility in the blends. TR polymers are typically insoluble and may form a crosslinked structure in the dispersed phase following heat treatment [31]. However, since the insoluble portion of the heat treated blends is 2–3 times greater than the amount of TR polymer present, crosslinking in the dispersed polyimide phase cannot fully explain the decreased solubility and increased gas selectivity. There must also be some insoluble regions forming in the PBI phase. The increase in selectivity is therefore likely due to changes in the continuous PBI phase during heat treatment at 400 °C, discussed later in this work, rather than the TR process in the dispersed polyimide phase. This hypothesis is further supported by Maxwell model predictions that changes in selectivity of immiscible blends would be primarily dictated by changes in the selectivity of the continuous phase.

A polymer's fractional free volume (FFV) can provide useful insight into its gas transport properties, since FFV represents the amount of unoccupied space between polymer chains available for gas diffusion [55,56]. Permeabilities often correlate exponentially with 1/FFV, and changes in FFV or chain packing are often reflected in gas permeabilities and selectivities [55,57,58]. Fractional free volumes were determined for Celazole® films cast with 1-methylimidazole with and without heat treatment as follows [59,60]:

$$FFV = 1 - 1.3\rho \sum \hat{V}_p^{vDw} \quad (1)$$

where ρ is the polymer density in g/cm^3, and $1.3 \sum \hat{V}_p^{vDw}$ is the volume occupied by polymer chains calculated from group contribution theory (0.693 cm^3/g for Celazole®). The density of Celazole® cast with 1-methylimidazole was 1.262 ± 0.007 g/cm^3, which corresponds to a FFV of 0.125 ± 0.001. This FFV is higher than the value previously measured for Celazole® without 1-methylimidazole added to the casting solution (FFV = 0.104) [11]. Since it is hypothesized that 1-methylimidazole evaporates during the initial solvent removal steps as the glassy film is being formed, this increase in FFV is consistent with the hypothesis that 1-methylimidazole leaves behind additional free volume when it evaporates, increasing permeabilities (cf., Fig. 9A). After 400 °C heat treatment, Celazole® density increased to 1.295 ± 0.008 g/cm^3, and FFV decreased to 0.103 ± 0.001. This reduction in free volume is consistent with a more densified, size-sieving structure that reduces permeabilities of larger gases (e.g., O_2 and CO_2) with less effect on smaller gases (e.g., H_2), thus increasing selectivities. PBI has a glass transition temperature between 400 and 450 °C, so heat treatment at 400 °C may provide enough thermal energy to anneal the polymer, relax out excess fractional free volume, and permit chain restructuring to form more highly ordered regions [61,62].

3.4. Small and wide angle x-ray scattering

Celazole® is thermally stable at temperatures as high as 550 °C with no observed mass loss in inert conditions [1,4]. However, previous studies have observed insolubility in PBIs heat treated at high temperatures (e.g., 450–500 °C) [63–65]. Crosslinking and/or chain scission are hypothesized to occur at these temperatures from free radical reactions [63,66]. While FTIR analysis has indicated chemical changes occur in PBI heated to temperatures as high as 350 °C in air, no changes in FTIR spectra have been observed for Celazole® heat treated under argon for 16 h at 400 °C [65,66]. Therefore, it is inconclusive whether thermally-induced crosslinking is occurring in these blends in either or both phases.

Another phenomenon may be contributing to decreased solubility in DMAc and increased gas selectivities for the heat treated PBI blends. Celazole® is known to be amorphous at room temperature [65]. When treated at temperatures around 350 °C, Celazole® exhibits an increase in structural order evidenced by x-ray scattering [65]. This increase in structural order has also been observed by FTIR to occur at temperatures at and above 400 °C, and an N—H stretching mode at 3420 cm^{-1} has been attributed to these para-crystalline domains [42]. Potentially, the presence of such additional structural order could impact properties such as solubility.

Both small angle x-ray scattering (SAXS) and wide angle x-ray scattering (WAXS) were measured for untreated and heat treated samples of Celazole® and HAB-6FDA-CI films cast with 1-methylimidazole and 20/80 and 33/67 wt% HAB-6FDA-CI/Celazole® compatibilized blends. Scattering intensities were normalized for film thickness to permit quantitative comparisons between samples. SAXS results are shown in Fig. 10. While no peaks were present in untreated films, consistent with their amorphous behavior, a peak emerged at around 0.29° for Celazole® and 0.38–0.42° for the 20 and 33% polyimide blends. Scattering peaks from crystalline regions in polyethylene, poly(butylene terephthalate), and polyoxymethylene have been reported between scattering angles of 0.3° and 0.7°, which are similar to the values of 0.3–0.4° observed in this study [67–69]. Although the SAXS peaks for heat treated Celazole® and polyimide/PBI blends are less intense and less sharp than those observed in semicrystalline polymers like polyethylene, this pattern nonetheless suggests the formation of some para-crystalline regions in Celazole® and in the PBI phase of the blends. No peak emerged in HAB-6FDA-CI after heat treatment, indicating the polyimide does not undergo the same structural ordering as PBI.

WAXS results for the same samples are shown in Fig. 11. The *d*-spacing has often been ascribed to intermolecular distance between polymer chains [70,71]. From the results in Fig. 11, *d*-spacing values were calculated using Bragg's relation [70]:

$$d = \frac{n\lambda}{2 \sin \theta} \tag{2}$$

where n is 1, λ is the x-ray wavelength (1.5404 Å for CuKα), d is the *d*-spacing in Å, and θ is the scattering angle at the center of a broad peak. Before heat treatment, a broad peak in Celazole® cast with 1-methylimidazole was previously observed at a *d*-spacing of 4.7 Å [42]. After

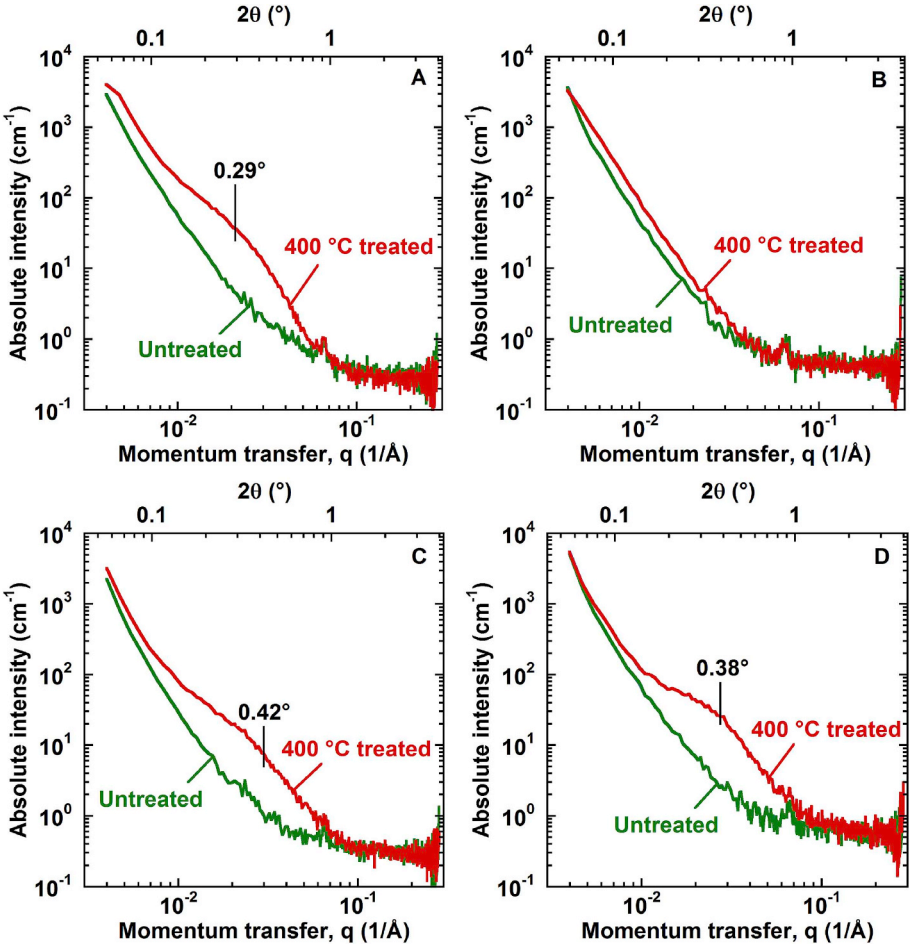

Fig. 10. Small angle x-ray scattering (SAXS) for: (A) Celazole® cast with 1-methylimidazole, (B) HAB-6FDA-CI cast with 1-methylimidazole, (C) 20/80 wt% HAB-6FDA-CI/Celazole® compatibilized blend, and (D) 33/67 wt% HAB-6FDA-CI/Celazole® compatibilized blend. Green curves are for untreated films, and red curves are for films treated at 400 °C. Intensities were corrected for film thicknesses to permit quantitative comparisons between samples. (For interpretation of the references to color in this figure legend, the reader is referred to the Web version of this article.)

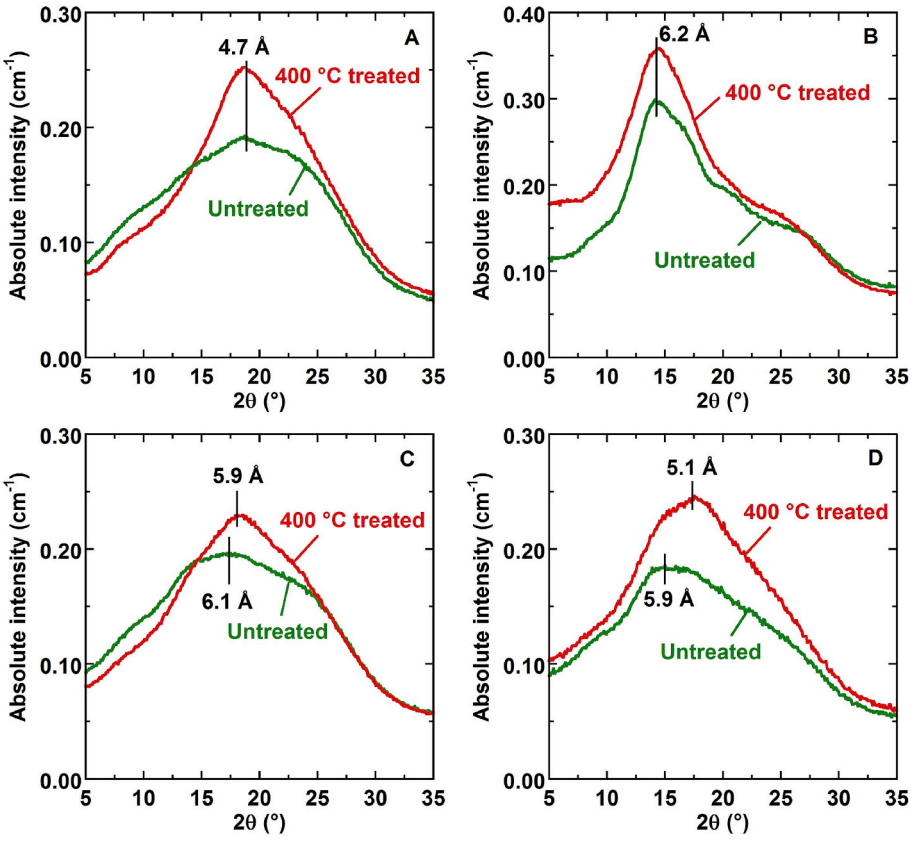

Fig. 11. Wide angle x-ray scattering (WAXS) for: (A) Celazole® cast with 1-methylimidazole [42], (B) HAB-6FDA-CI cast with 1-methylimidazole, (C) 20/80 wt% HAB-6FDA-CI/Celazole® compatibilized blend, and (D) 33/67 wt% HAB-6FDA-CI/Celazole® compatibilized blend. Green curves are for untreated films, and red curves are for films treated at 400 °C. Intensities were corrected for film thicknesses to permit quantitative comparisons between samples. (For interpretation of the references to color in this figure legend, the reader is referred to the Web version of this article.)

Table 1
Mechanical properties of Celazole® and heat treated 20/80 and 33/67 wt% HAB-6FDA-CI/Celazole® compatibilized blends. Mechanical properties of HAB-6FDA-CI before and after thermal rearrangement at 400 °C and Celazole® samples formed by compression-molding are provided for comparison [1,72].

Material	Young's modulus (GPa)	Elongation at break (%)	Ultimate tensile strength (MPa)	# samples
20/80 PI/PBI + 1-IM TR400	4.0 ± 0.5	3.0 ± 0.3	109 ± 6	3
33/67 PI/PBI + 1-IM TR400	3.9 ± 1.2	3.0 ± 0.4	110 ± 1	2
Celazole®	3.8 ± 0.4	–	94 ± 4	5
Compression-molded Celazole® [1]	5.7	1.8	100	–
HAB-6FDA-CI [72]	3.5	7.1	153	–
HAB-6FDA-CI TR400 [72]	2.5	4.0	85	–

heat treatment, this peak became much sharper, which was previously observed by Aili et al. for PBI treated for at least 10 min at 350 °C under argon [65]. This peak was centered around 19°, which is very close to the 2θ value of 18° reported previously [65]. Additionally, the absolute scattering intensity decreased at lower angles (i.e., higher *d*-spacings), which may indicate a narrowing of free volume distribution toward smaller free volume elements that would correspond with lower *d*-spacing. This result is also consistent with the observed reduction in FFV and increase in density for Celazole® after heat treatment.

An amorphous peak centered at a *d*-spacing of 6.2 Å was observed for HAB-6FDA-CI cast with 1-methylimidazole and its TR analog, which agrees with the previously reported *d*-spacing of 6.2 Å for the same polymer cast without 1-methylimidazole [38]. Amorphous peaks centered at *d*-spacing values of 6.1 and 5.9 Å were observed for the untreated 20/80 and 33/67 wt% HAB-6FDA-CI/Celazole® compatibilized blends, respectively. After heat treatment, these peaks became sharper and shifted to a slightly lower *d*-spacing of 5.9 Å for the 20% polyimide blend and to a rather lower *d*-spacing of around 5.1 Å for the 33% polyimide blend. After heat treatment, the 20% blend showed a decrease in absolute scattering intensities at higher *d*-spacing, similar to Celazole®, while the 33% blend showed an overall increase in absolute scattering intensity which was also observed for the HAB-6FDA-CI film. Scattering plots for 20/80 and 33/67 wt% HAB-6FDA-CI/Celazole® blends before and after heat treatment can be accurately reproduced ($R^2 > 0.98$) by superimposing scattering peaks of their pure polymer components weighted by their weight fractions in the blend (see supporting information).

The similar changes in the WAXS spectra for Celazole® and the 20% polyimide blend are consistent with the transport behavior of this blend composition being influenced by densification and ordering of the PBI phase. A reduction in free volume and a potential narrowing of the free volume distribution in the PBI phase from high temperature annealing reduced permeabilities of larger gases such as O_2 and CO_2 in the PBI matrix phase with less effect on smaller gases such as H_2. This behavior increased gas selectivities of the PBI matrix phase which, in turn, increased blend selectivity. As there was relatively little polyimide in this composition, the thermal rearrangement of the polyimide contributed little to the gas transport properties of the blend. Consequently, the gas permeabilities of Celazole® and the 20% polyimide blend were similar after heat treatment. On the other hand, the 33% polyimide blend exhibited higher gas permeabilities before and after heat treatment than Celazole® treated under the same conditions. The simultaneous increase in permeability and selectivity after heat treatment of the 33% blend occurred from the combination of increased permeability in the

dispersed polyimide phase from the TR reaction and increased selectivity in the PBI matrix phase from ordering and densification.

3.5. Mechanical properties

Tensile properties of pure Celazole® cast without 1-methylimidazole and heat treated 20/80 and 33/67 wt% HAB-6FDA-CI/Celazole® compatibilized blends were determined by testing microtensile samples on a universal tensile testing apparatus. Young's modulus, elongation at break, and ultimate tensile strength for these samples are summarized in Table 1. Untreated blend films with 20 or 33% polyimide were relatively brittle, and only a small fraction of die cut samples were useable. 50/50 wt% HAB-6FDA-CI/Celazole® blends were particularly brittle without heat treatment and consequently could not be tested for gas transport or mechanical properties. Elongation at break was not reported for Celazole® because samples failed by tearing, which yielded inaccurate elongation at break values.

The 20 and 33% polyimide heat treated blends exhibited a low elongation at break of 3.0% which was similar to that observed in thermally-rearranged HAB-6FDA-CI. TR polymers are typically brittle and prone to breaking upon bending [72]. While the heat treated blends in this study had low elongations at break, they exhibited higher elastic (Young's) moduli and ultimate tensile strengths than TR HAB-6FDA-CI which were comparable to those of Celazole®. Unlike TR HAB-6FDA-CI, the 20 and 33% polyimide heat treated blends were flexible enough to be bent 180° without breaking. Additional mechanical tests such as bending tests would be required to more fully understand the flexibility and mechanical behavior of these materials.

4. Conclusions

Phase separated blends of Celazole® PBI and *ortho*-functional HAB-6FDA-CI polyimide were prepared at compositions ranging from 20 to 80 wt% polyimide. The addition of 1-methylimidazole to casting solutions improved the compatibility of the two phases and resulted in a uniform, microscopically phase separated structure. Compatibilized blends containing 20 to 33 wt% polyimide had a continuous PBI matrix with submicron dispersions of polyimide. Heat treating these blends at 400 °C thermally rearranged the polyimide phase to a polybenzoxazole structure at similar conversion to that observed for the pure polyimide.

H_2/CO_2 selectivities at 35 °C for pure Celazole® and 20 to 33 wt% polyimide compatibilized blends increased after heat treatment due to densification and a decrease in free volume of the PBI matrix phase. Heat treatment also resulted in formation of para-crystalline regions in the PBI phase as evidenced by x-ray scattering. H_2 permeability increased after heat treatment for the 33% polyimide compatibilized blend, resulting in transport properties exceeding the 2008 upper bound for both 20 and 33% polyimide heat treated compatibilized blends. This behavior was due to the simultaneous densification of the PBI matrix phase that increased blend gas selectivity and thermal rearrangement of the dispersed polyimide phase that increased blend gas permeability.

Declarations of interest

None.

Funding

This work was supported by the U.S. Department of Energy Office of Science, Office of Basic Energy Sciences [grant number DE-FG02–02ER15362], the National Science Foundation Graduate Research Fellowship Program [grant number DGE-1610403], and the National Science Foundation [Cooperative Agreement No. EEC-1647722]. We gratefully acknowledge partial support of this work by the Australian-American Fulbright Commission for the award to B.D.F. of the U.S. Fulbright Distinguished Chair in Science, Technology and Innovation sponsored by the Commonwealth Scientific and Industrial Research Organization (CSIRO). Any opinions, findings, and conclusions or recommendations expressed in this material are those of the author(s) and do not necessarily reflect the views of the National Science Foundation.

Acknowledgements

The authors would like to acknowledge Michelle Dose for synthesizing HAB-6FDA-CI, Dr. Steve Swinnea for running WAXS and SAXS and providing data interpretation, Dr. Andrei Dolocan for providing SEM training, Dr. Rajkiran Tiwari for performing ultramicrotoming, and Dr. Karalee Jarvis for running TEM/STEM/EDS and providing data interpretation.

Appendix A. Supplementary data

Supplementary data to this article can be found online at https://doi.org/10.1016/j.memsci.2019.03.067.

References

[1] T.-S. Chung, A critical review of polybenzimidazoles, J. Macromol. Sci., Part C 37 (1997) 277–301.
[2] X. Li, R.P. Singh, K.W. Dudeck, K.A. Berchtold, B.C. Benicewicz, Influence of polybenzimidazole main chain structure on H_2/CO_2 separation at elevated temperatures, J. Membr. Sci. 461 (2014) 59–68.
[3] K.A. Berchtold, R.P. Singh, K.W. Dudeck, G.J. Dahe, C.F. Welch, D. Yang, High temperature polymer based membrane systems for pre-combustion carbon dioxide capture, NETL CO_2 Capture Technology Meeting, Pittsburgh, PA, 2012.
[4] S.C. Kumbharkar, Y. Liu, K. Li, High performance polybenzimidazole based asymmetric hollow fibre membranes for H_2/CO_2 separation, J. Membr. Sci. 375 (2011) 231–240.
[5] S.C. Kumbharkar, U.K. Kharul, Investigation of gas permeation properties of systematically modified polybenzimidazoles by N-substitution, J. Membr. Sci. 357 (2010) 134–142.
[6] D.R. Pesiri, B. Jorgensen, R.C. Dye, Thermal optimization of polybenzimidazole meniscus membranes for the separation of hydrogen, methane, and carbon dioxide, J. Membr. Sci. 218 (2003) 11–18.
[7] K.A. Berchtold, R.P. Singh, J.S. Young, K.W. Dudeck, Polybenzimidazole composite membranes for high temperature synthesis gas separations, J. Membr. Sci. 415–416 (2012) 265–270.
[8] T.C. Merkel, M. Zhou, R.W. Baker, Carbon dioxide capture with membranes at an IGCC power plant, J. Membr. Sci. 389 (2012) 441–450.
[9] S.H. Han, J.E. Lee, K.-J. Lee, H.B. Park, Y.M. Lee, Highly gas permeable and microporous polybenzimidazole membrane by thermal rearrangement, J. Membr. Sci. 357 (2010) 143–151.
[10] L.M. Robeson, The upper bound revisited, J. Membr. Sci. 320 (2008) 390–400.
[11] K.A. Stevens, H. Borjigin, J.D. Moon, R. Liu, R.M. Joseph, J.S. Riffle, B.D. Freeman, Influence of temperature on gas transport properties of tetraaminodiphenylsulfone (TADPS) based polybenzimidazoles, In preparation (2019).
[12] H. Borjigin, K.A. Stevens, R. Liu, J.D. Moon, A.T. Shaver, S. Swinnea, B.D. Freeman, J.S. Riffle, J.E. McGrath, Synthesis and characterization of polybenzimidazoles derived from tetraaminodiphenylsulfone for high temperature gas separation membranes, Polymer 71 (2015) 135–142.
[13] S.C. Kumbharkar, U.K. Kharul, New N-substituted ABPBI: synthesis and evaluation of gas permeation properties, J. Membr. Sci. 360 (2010) 418–425.
[14] T. Yang, Y. Xiao, T.-S. Chung, Poly-/metal- benzimidazole nano-composite membranes for hydrogen purification, Energy Environ. Sci. 4 (2011) 4171–4180.
[15] T. Yang, G.M. Shi, T.-S. Chung, Symmetric and asymmetric zeolitic imidazolate frameworks (ZIFs)/Polybenzimidazole (PBI) nanocomposite membranes for hydrogen purification at high temperatures, Adv. Energy Mater. 2 (2012) 1358–1367.
[16] T. Yang, T.-S. Chung, Room-temperature synthesis of ZIF-90 nanocrystals and the derived nano-composite membranes for hydrogen separation, J. Mater. Chem. A 1 (2013) 6081–6090.
[17] T. Yang, T.-S. Chung, High performance ZIF-8/PBI nano-composite membranes for high temperature hydrogen separation consisting of carbon monoxide and water vapor, Int. J. Hydrogen Energy 38 (2013) 229–239.
[18] G.M. Shi, H. Chen, Y.C. Jean, T.S. Chung, Sorption, swelling, and free volume of polybenzimidazole (PBI) and PBI/zeolitic imidazolate framework (ZIF-8) nano-composite membranes for pervaporation, Polymer 54 (2013) 774–783.
[19] S.S. Hosseini, M.M. Teoh, T.S. Chung, Hydrogen separation and purification in membranes of miscible polymer blends with interpenetration networks, Polymer 49 (2008) 1594–1603.
[20] N.P. Panapitiya, S.N. Wijenayake, Y. Huang, D. Bushdiecker, D. Nguyen, C. Ratanawanate, G.J. Kalaw, C.J. Gilpin, I.H. Musselman, K.J. Balkus, J.P. Ferraris, Stabilization of immiscible polymer blends using structure directing metal organic frameworks (MOFs), Polymer 55 (2014) 2028–2034.

[21] N.P. Panapitiya, Novel compatibilized immiscible polymer blend based membranes for gas separations, Dissertation at The University of Texas at Dallas, 2014.
[22] N.P. Panapitiya, S.N. Wijenayake, D.D. Nguyen, Y. Huang, I.H. Musselman, K.J. Balkus, J.P. Ferraris, Gas separation membranes derived from high-performance immiscible polymer blends compatibilized with small molecules, ACS Appl. Mater. Interfaces 7 (2015) 18618–18627.
[23] N.P. Panapitiya, S.N. Wijenayake, D. Nguyen, C. Karunaweera, Y. Huang, K. Balkus Jr., I. Musselman, J. Ferraris, Compatibilized immiscible polymer blends for gas separations, Materials 9 (2016) 643.
[24] Y. Huang, Immiscible polymer blend membranes for high pressure, high temperature H_2/CO_2 separation, Dissertation at The University of Texas at Dallas, 2016.
[25] K. Sejin, Effect of small molecules on membrane microstructure and gas separation properties, Master's thesis at The University of Texas at Dallas, 2016.
[26] J.P. Ferraris, N. Panapitiya, S. Wijenayake, I. Musselman, C. Karunaweera Jr, K.J. Balkus, Compatibilized immiscible polymer blends and molecular sieve membranes thereof, US Patent Application US 2016/0263534 A1, 2016.
[27] K. Chamaal, N.P. Panapitiya, Y. Huang, I.H. Musselman, K.J. Balkus, J.P. Ferraris, Thermally treated compatibilized immiscible polymer blends for high temperature, high pressure H_2 separation, 2017 ACS National Meeting, Washington, DC, August 23, 2017.
[28] A. Naderi, A. Asadi Tashvigh, T.-S. Chung, M. Weber, C. Maletzko, Molecular design of double crosslinked sulfonated polyphenylsulfone/polybenzimidazole blend membranes for an efficient hydrogen purification, J. Membr. Sci. 563 (2018) 726–733.
[29] R.P. Singh, X. Li, K.W. Dudeck, B.C. Benicewicz, K.A. Berchtold, Polybenzimidazole based random copolymers containing hexafluoroisopropylidene functional groups for gas separations at elevated temperatures, Polymer 119 (2017) 134–141.
[30] H.B. Park, C.H. Jung, Y.M. Lee, A.J. Hill, S.J. Pas, S.T. Mudie, E.V. Wagner, B.D. Freeman, D.J. Cookson, Polymers with cavities tuned for fast selective transport of small molecules and ions, Science 318 (2007) 254–258.
[31] D.F. Sanders, Z.P. Smith, C.P. Ribeiro Jr., R. Guo, J.E. McGrath, D.R. Paul, B.D. Freeman, Gas permeability, diffusivity, and free volume of thermally rearranged polymers based on 3,3′-dihydroxy-4,4′-diamino-biphenyl (HAB) and 2,2′-bis-(3,4-dicarboxyphenyl) hexafluoropropane dianhydride (6FDA), J. Membr. Sci. 409–410 (2012) 232–241.
[32] Y.M. Xu, N.L. Le, J. Zuo, T.-S. Chung, Aromatic polyimide and crosslinked thermally rearranged poly(benzoxazole-co-imide) membranes for isopropanol dehydration via pervaporation, J. Membr. Sci. 499 (2016) 317–325.
[33] Y. Zhuang, J.G. Seong, W.H. Lee, Y.S. Do, M.J. Lee, G. Wang, M.D. Guiver, Y.M. Lee, Mechanically tough, thermally rearranged (TR) random/block poly(benzoxazole-co-imide) gas separation membranes, Macromolecules 48 (2015) 5286–5299.
[34] G. Dong, Y. Moo Lee, Microporous polymeric membranes inspired by adsorbent for gas separation, J. Mater. Chem. A 5 (2017) 13294–13319.
[35] Y. Seong Do, W. Hee Lee, J. Geun Seong, J. Sung Kim, H. Hyun Wang, C.M. Doherty, A.J. Hill, Y. Moo Lee, Thermally rearranged (TR) bismaleimide-based network polymers for gas separation membranes, Chem. Commun. 52 (2016) 13556–13559.
[36] S.H. Han, H.J. Kwon, K.Y. Kim, J.G. Seong, C.H. Park, S. Kim, C.M. Doherty, A.W. Thornton, A.J. Hill, Á.E. Lozano, K.A. Berchtold, Y.M. Lee, Tuning microcavities in thermally rearranged polymer membranes for CO_2 capture, Phys. Chem. Chem. Phys. 14 (2012) 4365–4373.
[37] Y. Zhuang, J.G. Seong, Y.M. Lee, Polyimides containing aliphatic/alicyclic segments in the main chains, Prog. Polym. Sci. 92 (2019) 35–88.
[38] Z.P. Smith, D.F. Sanders, C.P. Ribeiro, R. Guo, B.D. Freeman, D.R. Paul, J.E. McGrath, S. Swinnea, Gas sorption and characterization of thermally rearranged polyimides based on 3,3′-dihydroxy-4,4′-diamino-biphenyl (HAB) and 2,2′-bis-(3,4-dicarboxyphenyl) hexafluoropropane dianhydride (6FDA), J. Membr. Sci. 415–416 (2012) 558–567.
[39] J.D. Moon, M. Galizia, H. Borjigin, R. Liu, J.S. Riffle, B.D. Freeman, D.R. Paul, Water vapor sorption, diffusion, and dilation in polybenzimidazoles, Macromolecules 51 (2018) 7197–7208.
[40] D. Halliday, R. Resnick, J. Walker, Fundamentals of Physics, John Wiley & Sons, 2010.
[41] H. Lin, B.D. Freeman, Permeation and diffusion, in: H. Czichos, L.E. Smith, T. Saito (Eds.), Springer Handbook of Material Measurement Methods, Springer, New York, 2006, pp. 371–387.
[42] P. Musto, P. La Manna, J.D. Moon, M. Galizia, B.D. Freeman, Infrared spectroscopy of polybenzimidazole in the dry and hydrate forms: a combined experimental and computational study, ACS Omega 3 (2018) 11592–11607.
[43] M. Yousfi, S. Livi, J. Duchet-Rumeau, Ionic liquids: a new way for the compatibilization of thermoplastic blends, Chem. Eng. J. 255 (2014) 513–524.
[44] D. Broseta, L. Leibler, L. Ould Kaddour, C. Strazielle, A theoretical and experimental study of interfacial tension of immiscible polymer blends in solution, J. Chem. Phys. 87 (1987) 7248–7256.
[45] C. Konak, P. Stepanek, P. Vlcek, R.M. Johnsen, Phase separation in concentrated solutions of two homopolymers and a diblock copolymer, Macromolecules 28 (1995) 2852–2857.
[46] L. Sung, C.C. Han, Light-scattering studies on phase separation in a binary blend with addition of diblock copolymers, J. Polym. Sci. B Polym. Phys. 33 (1995) 2405–2412.
[47] D.F. Sanders, R. Guo, Z.P. Smith, Q. Liu, K.A. Stevens, J.E. McGrath, D.R. Paul, B.D. Freeman, Influence of polyimide precursor synthesis route and ortho-position functional group on thermally rearranged (TR) polymer properties: conversion and free volume, Polymer 55 (2014) 1636–1647.
[48] L.M. Robeson, Polymer blends in membrane transport processes, Ind. Eng. Chem. Res. 49 (2010) 11859–11865.
[49] J.H. Petropoulos, A comparative study of approaches applied to the permeability of binary composite polymeric materials, J. Polym. Sci. Polym. Phys. Ed 23 (1985) 1309–1324.
[50] H.B. Hopfenberg, D.R. Paul, Transport phenomena in polymer blends, in: D.R. Paul, S. Newman (Eds.), Polymer Blends, Academic Press, Inc., New York, 1978, pp. 445–489.
[51] G.S. Narang, J.D. Moon, W. Zhang, G.C. Miller, S.R. Choudhury, A. Shaver, B. Vondrasek, J.J. Lesko, J.J. Fallon, M. Bortner, C. D'Ambra, B.D. Freeman, J.S. Riffle, Synthesis and characterization of a phosphine oxide based poly(arylene ether ketone) and blends with poly(2,6-dimethyl-1,4-phenylene oxide) for gas separations, Polymer 138 (2018) 156–168.
[52] A. Morisato, H.C. Shen, S.S. Sankar, B.D. Freeman, I. Pinnau, C.G. Casillas, Polymer characterization and gas permeability of poly(1-trimethylsilyl-1-propyne) [PTMSP], poly(1-phenyl-1-propyne) [PPP], and PTMSP/PPP blends, J. Polym. Sci. B Polym. Phys. 34 (1996) 2209–2222.
[53] E.V. Perez, K.J. Balkus, I.H. Musselman, Improvement of gas separation properties of polybenzimidazole membranes for gas separations at high pressure and high temperature through thermal treatment, Prepr. Pap.-Am. Chem. Soc., Div. Energy Fuels 61 (2016) 208.
[54] S.C. Kumbharkar, K. Li, Structurally modified polybenzimidazole hollow fibre membranes with enhanced gas permeation properties, J. Membr. Sci. 415–416 (2012) 793–800.
[55] M.H. Cohen, D. Turnbull, Molecular transport in liquids and glasses, J. Chem. Phys. 31 (1959) 1164–1169.
[56] K. Ghosal, B.D. Freeman, Gas separation using polymer membranes: an overview, Polym. Adv. Technol. 5 (1993) 673–697.
[57] D.F. Sanders, Z.P. Smith, R. Guo, L.M. Robeson, J.E. McGrath, D.R. Paul, B.D. Freeman, Energy-efficient polymeric gas separation membranes for a sustainable future: a review, Polymer 54 (2013) 4729–4761.
[58] M.C. Ferrari, M. Galizia, M.G. De Angelis, G.C. Sarti, Gas and vapor transport in mixed matrix membranes based on amorphous teflon AF1600 and AF2400 and fumed silica, Ind. Eng. Chem. Res. 49 (2010) 11920–11935.
[59] J.Y. Park, D.R. Paul, Correlation and prediction of gas permeability in glassy polymer membrane materials via a modified free volume based group contribution method, J. Membr. Sci. 125 (1997) 23–39.
[60] A. Bondi, van der Waals volumes and radii, J. Phys. Chem. 68 (1964) 441–451.
[61] J.D. Menczel, Thermal measurements on poly[2,2'-(m-phenylene)-5,5'-bibenzimidazole] fibers, J. Therm. Anal. Calorim. 59 (2000) 1023–1027.
[62] C. Arrieta, E. David, P. Dolez, T. Vu-Khanh, X-ray diffraction, Raman, and differential thermal analyses of the thermal aging of a Kevlar®-PBI blend fabric, Polym. Compos. 32 (2011) 362–367.
[63] H. Vogel, C.S. Marvel, Polybenzimidazoles, new thermally stable polymers, J. Polym. Sci. 50 (1961) 511–539.
[64] J.K. Gillham, Polymer structure: cross-linking of a polybenzimidazole, Science 139 (1963) 494–495.
[65] D. Aili, L.N. Cleemann, Q. Li, J. Oluf Jensen, E. Christensen, N.J. Bjerrum, Thermal curing of PBI membranes for high temperature PEM fuel cells, J. Mater. Chem. 22 (2012) 5444–5453.
[66] P. Musto, F.E. Karasz, W.J. MacKnight, Fourier transform infra-red spectroscopy on the thermo-oxidative degradation of polybenzimidazole and of a polybenzimidazole/polyetherimide blend, Polymer 34 (1993) 2934–2945.
[67] R. Crist, N. Morisoff, Small-angle X-ray scattering of semicrystalline polymers. II. Analysis of experimental scattering curves, J. Polym. Sci. Polym. Phys. Ed 11 (1973) 1023–1045.
[68] I.H. Hall, E.A. Mahmoud, P.D. Carr, Y.D. Geng, Small-angle-X-ray scattering by crystalline polymer fibres 1. Experimental method and investigation of the linear paracrystalline model, Colloid Polym. Sci. 265 (1987) 383–393.
[69] H. Hama, K. Tashiro, Structural changes in isothermal crystallization process of polyoxymethylene investigated by time-resolved FTIR, SAXS and WAXS measurements, Polymer 44 (2003) 6973–6988.
[70] A. Morisato, N.R. Miranda, B.D. Freeman, H.B. Hopfenberg, G. Costa, A. Grosso, S. Russo, The influence of chain configuration and, in turn, chain packing on the sorption and transport properties of poly(tert-butyl acetylene), J. Appl. Polym. Sci. 49 (1993) 2065–2074.
[71] S. Luo, Q. Zhang, T.K. Bear, T.E. Curtis, R.K. Roeder, C.M. Doherty, A.J. Hill, R. Guo, Triptycene-containing poly(benzoxazole-co-imide) membranes with enhanced mechanical strength for high-performance gas separation, J. Membr. Sci. 551 (2018) 305–314.
[72] Q. Liu, D.R. Paul, B.D. Freeman, Gas permeation and mechanical properties of thermally rearranged (TR) copolyimides, Polymer 82 (2016) 378–391.